

## Facile synthesis of $\text{ZnIn}_2\text{S}_4/\text{Cu}_2\text{O}$ hierarchical heterostructures for enhanced selectivity and sensitivity of $\text{NH}_3$ gas at room temperature

Bedala, Kranthi Kumar; Gonugunta, Prasad; Soleimani, Mohammad; Má dai, Eszter; Taheri, Peyman; Padamati, Sandeep Kumar; Nagaraju, P.; Upender, G.; Vijaya Kumar, B.

### DOI

[10.1016/j.apsusc.2023.158315](https://doi.org/10.1016/j.apsusc.2023.158315)

### Publication date

2023

### Document Version

Final published version

### Published in

Applied Surface Science

### Citation (APA)

Bedala, K. K., Gonugunta, P., Soleimani, M., Má dai, E., Taheri, P., Padamati, S. K., Nagaraju, P., Upender, G., & Vijaya Kumar, B. (2023). Facile synthesis of  $\text{ZnIn}_2\text{S}_4/\text{Cu}_2\text{O}$  hierarchical heterostructures for enhanced selectivity and sensitivity of  $\text{NH}_3$  gas at room temperature. *Applied Surface Science*, 640, Article 158315. <https://doi.org/10.1016/j.apsusc.2023.158315>

### Important note

To cite this publication, please use the final published version (if applicable).  
Please check the document version above.

### Copyright

Other than for strictly personal use, it is not permitted to download, forward or distribute the text or part of it, without the consent of the author(s) and/or copyright holder(s), unless the work is under an open content license such as Creative Commons.

### Takedown policy

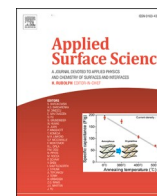
Please contact us and provide details if you believe this document breaches copyrights.  
We will remove access to the work immediately and investigate your claim.

***Green Open Access added to TU Delft Institutional Repository***

***'You share, we take care!' - Taverne project***

**<https://www.openaccess.nl/en/you-share-we-take-care>**

Otherwise as indicated in the copyright section: the publisher is the copyright holder of this work and the author uses the Dutch legislation to make this work public.



## Full Length Article

Facile synthesis of  $\text{ZnIn}_2\text{S}_4/\text{Cu}_2\text{O}$  hierarchical heterostructures for enhanced selectivity and sensitivity of  $\text{NH}_3$  gas at room temperatureKranthi Kumar Bedala<sup>a</sup>, Prasad Gonugunta<sup>b</sup>, Mohammad Soleimani<sup>b</sup>, Eszter Máda<sup>b</sup>, Peyman Taheri<sup>b</sup>, Sandeep Kumar Padamati<sup>c</sup>, P. Nagaraju<sup>d</sup>, G. Upender<sup>e,\*</sup>, B. Vijaya Kumar<sup>a,\*</sup><sup>a</sup> Department of Chemistry, Osmania University, Hyderabad, Telangana-500007, India<sup>b</sup> Materials Science and Engineering, Faculty of Mechanical, Maritime and Materials Engineering, Delft University of Technology, Mekelweg 2, 2628 CD Delft, the Netherlands<sup>c</sup> Department of Chemistry, University College London, 20 Gordon St, London WC1H 0AJ, United Kingdom<sup>d</sup> Department of Physics, Srinidhi University, Ghatkesar, Hyderabad, Telangana-501301, India<sup>e</sup> Department of Physics, Osmania University, Hyderabad, Telangana-500007, India

## ARTICLE INFO

## Keywords:

 $\text{ZnIn}_2\text{S}_4$  $\text{Cu}_2\text{O}$ 

p-n heterojunction

HRTEM

Chemoresistance

 $\text{NH}_3$  sensor

## ABSTRACT

The development of an effective and reliable sensor with the capability to detect ammonia ( $\text{NH}_3$ ) gas at room temperature exerts a significant influence on the sensor industry. The gas sensing performance is notably improved by the formation of a heterostructure between metal oxide with metal sulfides. In this study, pure  $\text{ZnIn}_2\text{S}_4$  (ZIS),  $\text{Cu}_2\text{O}$  and heterostructures of ZIS with 5, 10 and 20 wt% of  $\text{Cu}_2\text{O}$  were successfully prepared using hydrothermal, co-precipitation and heat treatment methods, respectively. A thorough investigation has been carried out to examine the sensing capabilities of all the materials upon exposure to  $\text{NH}_3$  with different concentrations (1, 5, 10, 15, 20, 25 and 50 ppm) at room temperature (RT). Impressively, the composite material  $0.9\text{ZnIn}_2\text{S}_4/0.1\text{Cu}_2\text{O}$  (ZIS-10) has exhibited remarkable gas sensitivity compared to pristine ZIS and  $\text{Cu}_2\text{O}$  towards 25 ppm  $\text{NH}_3$ , low limit of detection (1 ppm) with fast response/recovery times (37/25 sec). The improved performance of the ZIS-10 composite sensor may be ascribed to the synergistic effect between ZIS and  $\text{Cu}_2\text{O}$ , which facilitates the electron transfer from ZIS to the  $\text{Cu}_2\text{O}$  at the interface. The plausible gas-sensing mechanism and the pathways responsible for enhanced sensing are also discussed in detail.

## 1. Introduction

The developments in the industry have been indubitably improving the quality of societal needs, nevertheless, they show the detrimental effect on both the environment and human health. Chemical industries, agricultural operations, and vehicle exhaust emissions release hazardous gases viz. ammonia ( $\text{NH}_3$ ), benzene ( $\text{C}_6\text{H}_6$ ), formaldehyde ( $\text{CH}_2\text{O}$ ), hydrogen sulfide ( $\text{H}_2\text{S}$ ), toluene ( $\text{C}_6\text{H}_5\text{CH}_3$ ), xylene ( $\text{C}_6\text{H}_4(\text{CH}_3)_2$ ) and nitrogen dioxide ( $\text{NO}_2$ ).  $\text{NH}_3$  in particular, is one with very high toxicity and poisonous gas that is frequently used in many important technological areas including chemical engineering, food technology, fire-power plants, and medical diagnosis. Prolonged exposure to ammonia in the air has been having negative effects on the respiratory and cardiovascular systems. The recent ammonia gas explosion in West Texas resulted in the deaths of 15 individuals and over 260 injuries [1]. As such, the development of low-concentration detection methods for

ammonia gas in the air, plays an important role in medical applications, environmental protection and saving human lives.

Recently, significant research efforts have been directed towards the comprehensive exploration of diverse nanostructured materials for ammonia detection. These investigations aim to attain exceptional selectivity, heightened sensitivity, prompt response, minimal recovery time and remarkable stability in the realm of ammonia detection applications. Among the various types of gas sensors, metal oxide semiconductors (MOS), for instance n-type materials i.e.  $\text{WO}_3$  [2–7],  $\text{In}_2\text{O}_3$  [8–15],  $\text{SnO}_2$  [16–19],  $\text{ZnO}$  [20–22],  $\text{TiO}_2$  [23,24],  $\text{Fe}_2\text{O}_3$  [25,26] and p-type materials i.e.  $\text{MoO}_3$  [27],  $\text{NiO}$  [28–30],  $\text{CuO}$  [31,32] and  $\text{Cu}_2\text{O}$  [33,34] have been established as leading sensors for the gas detection owing to their excellent properties like outstanding sensitivity, good response/recovery, chemical and thermal stability etc. Cuprous oxide ( $\text{Cu}_2\text{O}$ ) is an important p-type metal oxide semiconductor (1.9–2.2 eV) which exhibits extraordinary catalytic abilities and gas-sensing

\* Corresponding authors.

E-mail addresses: [upenderg@osmania.ac.in](mailto:upenderg@osmania.ac.in) (G. Upender), [vijaychemou@osmania.ac.in](mailto:vijaychemou@osmania.ac.in) (B. Vijaya Kumar).<https://doi.org/10.1016/j.apsusc.2023.158315>

Received 24 May 2023; Received in revised form 31 July 2023; Accepted 22 August 2023

Available online 22 August 2023

0169-4332/© 2023 Elsevier B.V. All rights reserved.

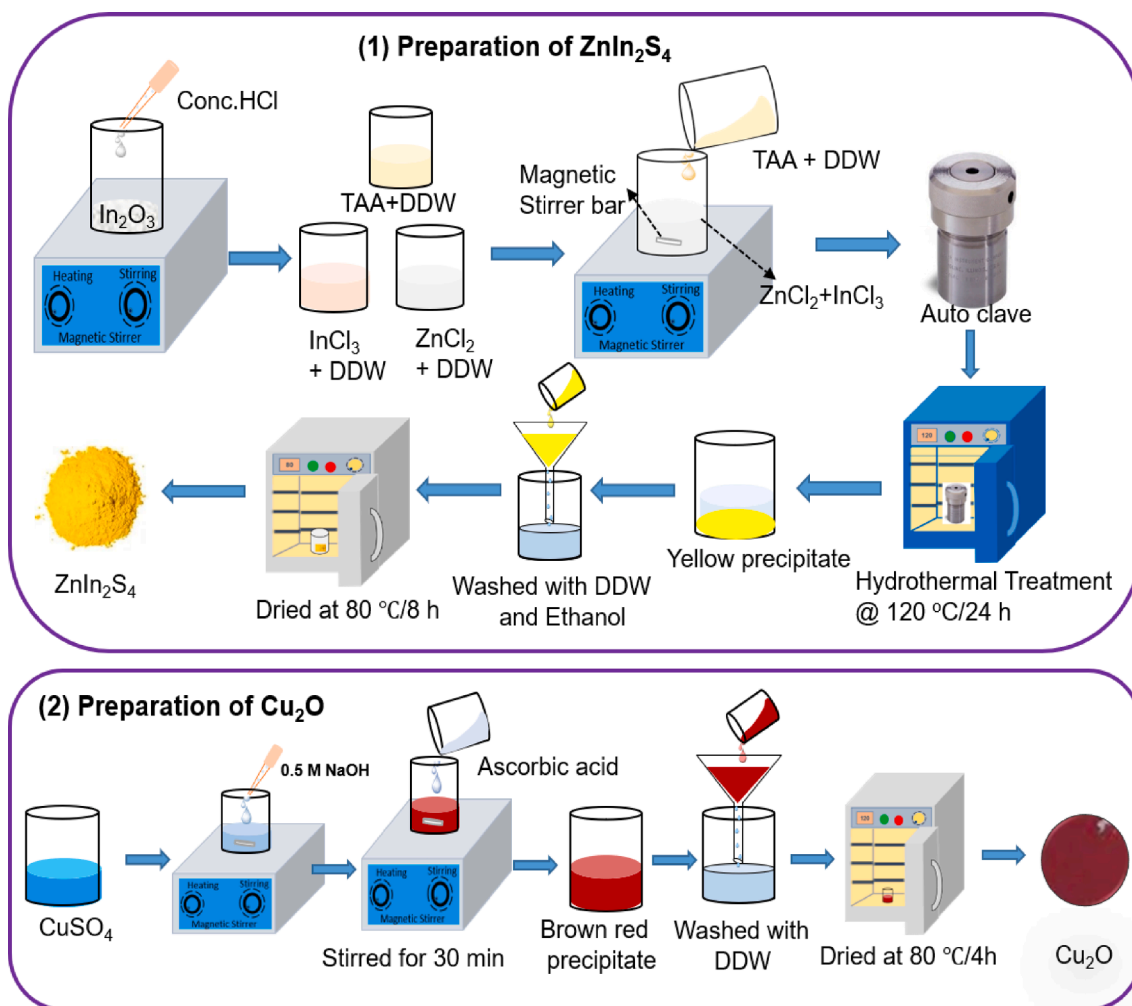


Fig. 1. Schematic illustration for the preparation of  $\text{ZnIn}_2\text{S}_4$  micro flowers and  $\text{Cu}_2\text{O}$  hexapods.

properties [35,36]. In general, p-type  $\text{Cu}_2\text{O}$  resistance rises resulting from free electrons being released by the adsorbed oxygen to the conduction band, rendering it difficult to measure. Hence, to reduce the resistance of a gas sensor some other materials are composited with  $\text{Cu}_2\text{O}$  to form composites [37]. For instance, Ding et al. [38] synthesized  $\text{Cu}_2\text{O}/\text{MoS}_2$ , p-p type heterostructure and investigated the  $\text{NH}_3$  sensing of 20–100 parts per million (ppm). Ranjan Kumar et al. [39] examined the  $\text{NO}_2$  sensing capabilities under 254 nm UV irradiation in the presence of  $\text{MOS}_2/\text{Cu}_2\text{O}/\text{ZnO}$  heterostructure and found that MCZ45 exhibited superior sensitivity compared to  $\text{Cu}_2\text{O}/\text{ZnO}$ . Additionally, the gas sensing capabilities of  $\text{Cu}_2\text{O}$  are not well understood, and a more extensive study is imperative to optimize its gas sensing properties and elucidate its operating mechanism. Hence, the development of heterostructure between  $\text{Cu}_2\text{O}$  and other metal oxides/sulfides emerges as a promising approach to enhance the sensitivity of  $\text{Cu}_2\text{O}$  sensing performance.

In addition to metal oxides, the exploration of metal sulfides with layered structures has gained attention in the field of gas sensors because of their myriad advantages such as high surface area, ease of preparation, non-toxicity and large amount of sulfur vacancies. One such metal sulfide is zinc indium sulfide ( $\text{ZnIn}_2\text{S}_4$ ), which possesses a unique combination of physicochemical properties that render it as an attractive material for gas sensing applications.  $\text{ZnIn}_2\text{S}_4$  is a ternary n-type semiconductor (2.3 eV) [40], which exhibits remarkable gas sensing capabilities due to its two-dimensional (2D) layered hexagonal structure with a large surface area and S-vacancies [41]. Furthermore,  $\text{ZnIn}_2\text{S}_4$  is highly

stable both thermally and chemically, non-toxic, and inexpensive. However, despite its potential, there are relatively few studies on the gas-sensing properties of  $\text{ZnIn}_2\text{S}_4$ . Liu et al. [42] have improved the ethanol sensing of  $\text{ZnIn}_2\text{S}_4$  nanosheets coated on  $\text{In}_2\text{O}_3$  nanospheres. Fan et al. [43] have synthesized the sulfur vacancy-rich  $\text{ZnIn}_2\text{S}_4$  and studied the triethylamine sensing properties at room temperature (RT). According to us, the existing literature provides the most up-to-date on the gas-sensing properties of  $\text{ZnIn}_2\text{S}_4$ . Considering the preceding discussion, doping a metal into a semiconductor and/or the formation of a heterostructure is a highly efficient method for enhancing the sensitivity of a gas sensor. Among the above methods, we have chosen the latter because of the following reasons: (1) The formation of heterostructures between metal oxides and mesoporous 2D metal sulfides provides a large surface area for a reaction and (2) the chemical bonds formed between the materials can serve as charge transfer pathways during the gas-sensing process [44].

Thus, the present work aims to synthesize 2D  $\text{ZnIn}_2\text{S}_4$  hierarchical micro flowers and  $\text{Cu}_2\text{O}$  hexapods by hydrothermal and reductive solution methods respectively. The  $\text{NH}_3$  gas sensing performance, response/recovery times and limit of detection of pure materials and heterostructures were investigated to manifest the superior activity of  $\text{NH}_3$  detecting ability at RT. It was found that  $0.9\text{ZnIn}_2\text{S}_4/0.1\text{Cu}_2\text{O}$  (ZIS-10) nanocomposite exhibited excellent gas sensing properties compared to other compositions. The reasons for the enhanced gas sensing performance were explained with a plausible mechanism. This type of work bridges the knowledge gap and explores the potential of  $\text{ZnIn}_2\text{S}_4$  with p-



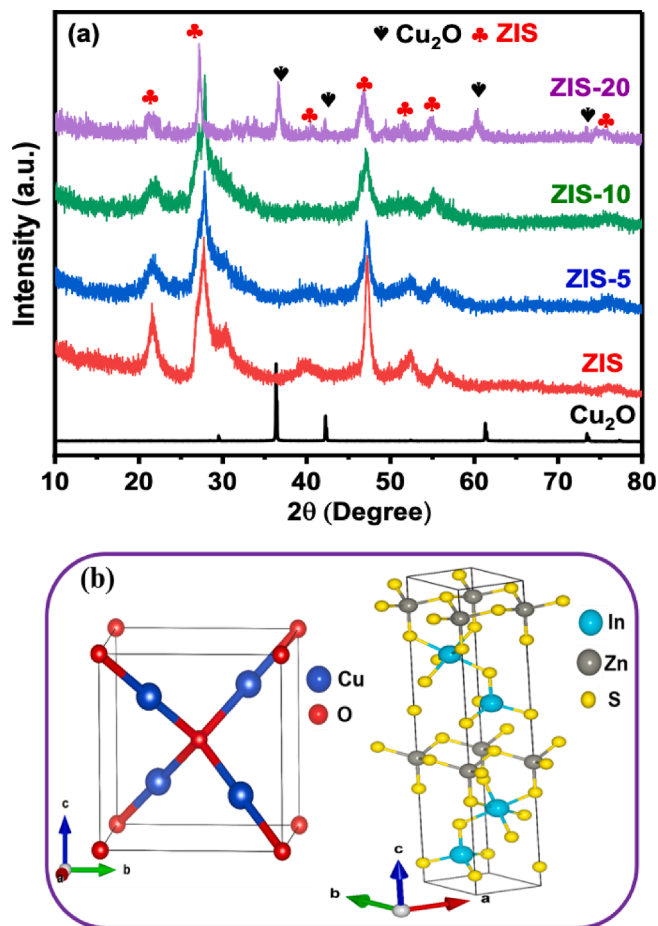


Fig. 2. (a) Powder XRD patterns of  $\text{Cu}_2\text{O}$ , ZIS-5, ZIS-10 and ZIS-20 (b) Unit cells of  $\text{ZnIn}_2\text{S}_4$  and  $\text{Cu}_2\text{O}$  by VESTA.

Table 1

Crystallite size, dislocation density and strain of all the materials.

S.No.	Crystallite size (nm)	Dislocation Density (Lines/m <sup>2</sup> )	Strain
$\text{Cu}_2\text{O}$	47.2	$0.08 \times 10^{-2}$	$0.044 \times 10^{-3}$
ZIS	6.9	$2.8 \times 10^{-2}$	$5.6 \times 10^{-3}$
ZIS-5	6.7	$3.2 \times 10^{-2}$	$5.9 \times 10^{-3}$
ZIS-10	6.5	$4.2 \times 10^{-2}$	$6.5 \times 10^{-3}$
ZIS-20	6.4	$4.9 \times 10^{-2}$	$6.9 \times 10^{-3}$

type semiconductors in gas sensing applications and the development of new metal sulfide-based gas sensors with improved sensitivity and selectivity.

## 2. Experimental section

### 2.1. Materials

The following chemicals were procured for the experiment: zinc chloride ( $\text{ZnCl}_2$ , 98%), thioacetamide (TAA, 98%), hydrochloric acid (HCl),  $\text{CuSO}_4 \cdot 5\text{H}_2\text{O}$ , NaOH, ascorbic acid and ethanol from SD fine chemicals.  $\text{In}_2\text{O}_3$  (99.5%) was obtained from Sigma Aldrich. All the chemicals are used in their received form without additional purification.

### 2.2. Preparation of flower-like $\text{ZnIn}_2\text{S}_4$ microspheres

$\text{ZnIn}_2\text{S}_4$  (ZIS) was synthesized using the hydrothermal method. In

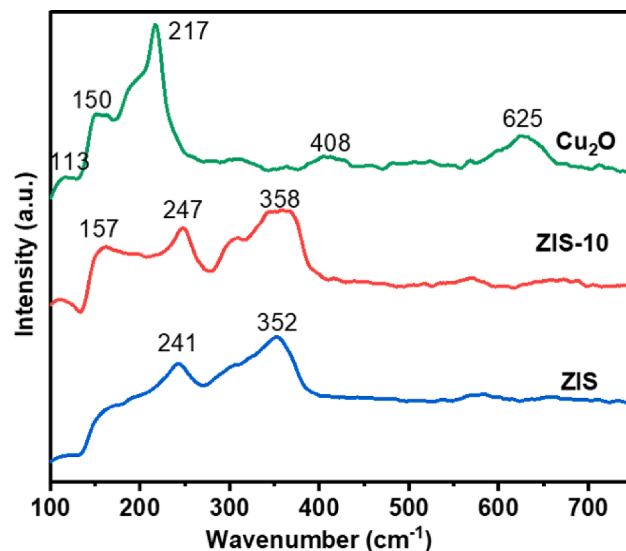


Fig. 3. Raman spectra of ZIS, ZIS-10 and  $\text{Cu}_2\text{O}$ .

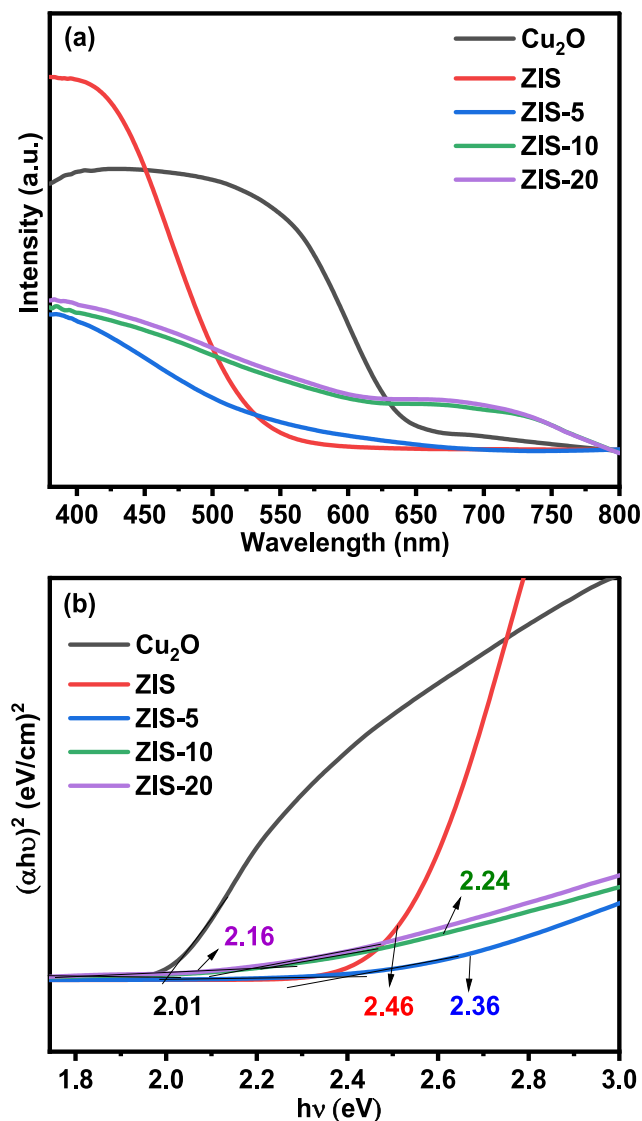


Fig. 4. (a) UV-Vis DRS spectra and (b) Tauc plot of all the compositions.

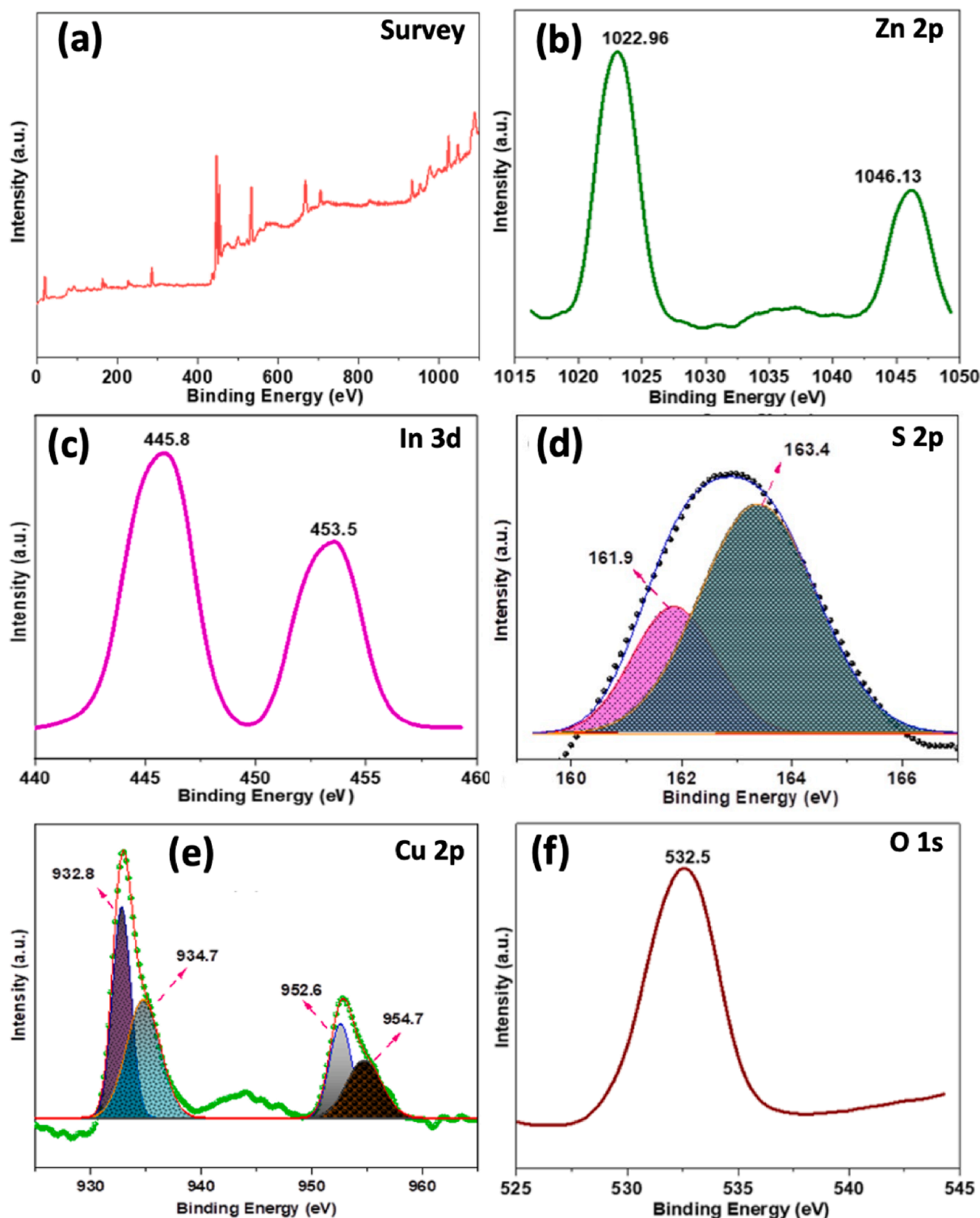


Fig. 5. XPS spectra (a) survey spectrum of ZIS-10, (b) Zn 2p, (c) In 3d, (d) S 2p, (e) Cu 2p, and (f) O 1s.

brief, stoichiometric amounts of  $\text{ZnCl}_2$  (0.02 mmol) and thioacetamide (0.08 mmol) were dissolved separately in 30 mL of distilled water. To obtain water-soluble  $\text{InCl}_3$ , the compound  $\text{In}_2\text{O}_3$  (0.02 mmol) was dissolved in conc. HCl and the excess HCl was evaporated on a hot plate. The attained white crystals ( $\text{InCl}_3$ ) were dissolved in distilled water. After adding the  $\text{ZnCl}_2$  solution to the  $\text{InCl}_3$  solution, the TAA solution was slowly added, and the resulting mixture was stirred for approximately 30 min. The obtained solution was transferred to a Teflon-lined stainless-steel autoclave and heated at  $120^\circ\text{C}$  in a hot air oven for 20 h.

After the formation of a yellow precipitate, it was washed three times distilled with water and subsequently rinsed three times with ethanol. Finally, the precipitate was dried at  $80^\circ\text{C}$  for 8 h.

### 2.3. Preparation of $\text{Cu}_2\text{O}$

To prepare  $\text{Cu}_2\text{O}$ , a co-precipitation method was employed. Typically, in a beaker 0.5 M  $\text{CuSO}_4 \cdot 5\text{H}_2\text{O}$  (25 mL) was taken, and then 0.5 M NaOH (20 mL) was slowly added drop by drop. This was followed by the

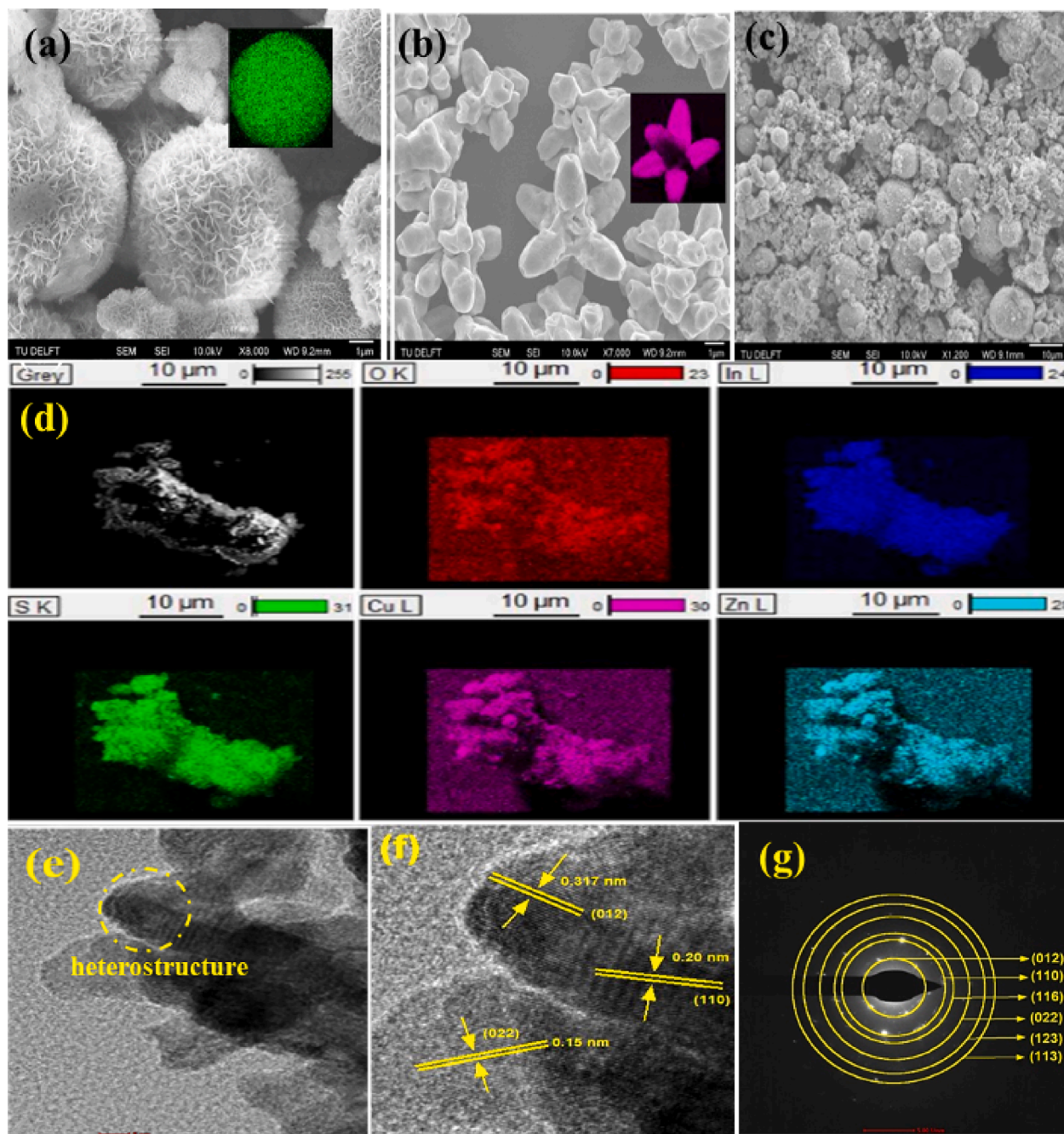


**Fig. 6.** FESEM images of (a) ZIS, (b)  $\text{Cu}_2\text{O}$ , (c) ZIS-10, and (d) color mapping of Zn, In, Cu, S and O and HRTEM images of (e) ZIS-10 heterostructure (f) high-resolution TEM images of ZIS-10 (lattice fringes) and (g) SAED pattern.

addition of 0.1 M ascorbic acid (25 mL), while continuously stirring the mixture for approximately about 30 min at room temperature (RT). The resulting precipitate, which appeared as a brownish red color, was washed with distilled water and ethanol 3–5 times. Subsequently, the precipitate was heated at 80 °C for 4 h. For visual clarity, the synthesis procedures of  $\text{ZnIn}_2\text{S}_4$  and  $\text{Cu}_2\text{O}$  are illustrated schematically in Fig. 1.

#### 2.4. Preparation of $\text{ZnIn}_2\text{S}_4/\text{Cu}_2\text{O}$ heterostructures

The  $\text{ZnIn}_2\text{S}_4/\text{Cu}_2\text{O}$  composites were prepared by the simple heat treatment method. For instance, to prepare 5 wt% of  $\text{Cu}_2\text{O}$  in  $\text{ZnIn}_2\text{S}_4$ , 5 mg of  $\text{Cu}_2\text{O}$  was added to the 95 mg of pure  $\text{ZnIn}_2\text{S}_4$  and ground thoroughly for 30 min. Afterwards, the resultant powder was taken into a silica crucible and heated in a furnace at 400 °C in the air for 2 h. After

natural cooling down to RT, the samples were collected and ground thoroughly for 30 min. A similar procedure was also adopted for the remaining samples and all the obtained composites of 5, 10 and 20 wt% of  $\text{Cu}_2\text{O}$  in  $\text{ZnIn}_2\text{S}_4$  were abbreviated as ZIS-5, ZIS-10 and ZIS-20 respectively. The details of all the characterization techniques have been given in electronic [supplementary information](#) (ESI).

#### 2.5. Gas sensor fabrication and measurement

The gas sensors were fabricated by a simple doctor blade method. Typically, 10 mg of each material was added with a few drops of acetone to make a slurry. The obtained slurry was uniformly coated on a 3 × 3 cm transparent glass slide, which was priorly cleaned with acetone, and dried at 80 °C. Afterwards, the electrodes were made by coating silver



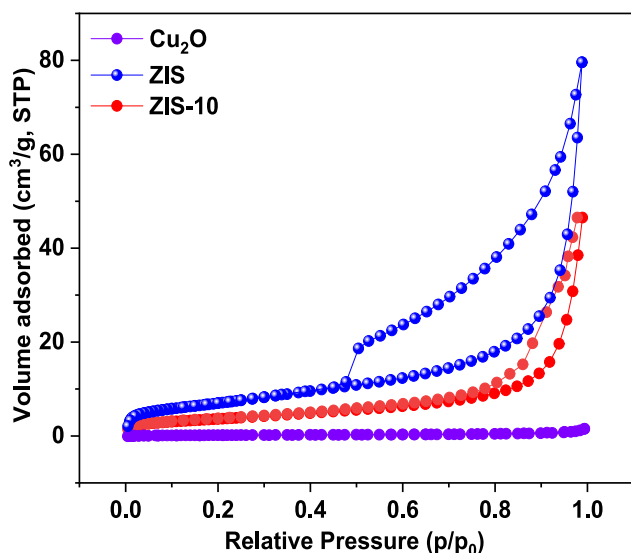


Fig. 7. BET surface area of ZIS, Cu<sub>2</sub>O and ZIS-10.

paste on both edges of the substrate and dried at 120 °C for 4 h. Later this thin layer coated plate is transformed into a gas sensing chamber. Initially, the resistance of the ZnIn<sub>2</sub>S<sub>4</sub>/Cu<sub>2</sub>O thin layer is measured in dry airflow to establish a baseline, after that the analyte gas is injected into the gas chamber and sealed then the resistance of the thin layer changes noticeably. The resistance ( $R_g$ ) of the sensor in the presence of analyte gas at different concentrations and the resistance ( $R_a$ ) of the sensor in the presence of dry air at room temperature were measured. The relative humidity in the chamber was maintained at 60% using a digital humidity controller (Humitherm, India). The gas instrument setup was provided in the ESI (Fig.S1).

### 3. Results and discussion

#### 3.1. Powder X-ray diffraction analysis

The phase composition and crystal structure of pure ZIS, Cu<sub>2</sub>O, and composites were examined by powder X-ray diffraction, and the results are displayed in Fig. 2(a). The pure ZIS shows prominent diffraction peaks at  $2\theta$  values, 21.5°, 27.7°, 30.3°, 39.7°, 47.3°, 52.3° and 55.4°, corresponding to the planes of (006), (012), (104), (108), (110), (116) and (022), respectively. The diffraction peaks are well consistent with the previous reports [42]. These observations imply that ZIS is crystallized in a hexagonal structure (JCPDS No. 98-000-4012) with space group P6<sub>3</sub>mc [43]. The absence of additional peaks in XRD patterns suggests the single phase of the prepared compound. The more intense and broadness of XRD peaks emphasize that the compound is comprised of crystals in the nanoscale. Likewise, the diffraction peaks of Cu<sub>2</sub>O hexapods were noticed at 29.5°, 36.4°, 42.2°, 61.2° and 73.5°. These peaks are correlated well with the planes of (011), (111), (002), (022) and (113), respectively. It indicates that Cu<sub>2</sub>O is crystallized in a cubic structure (JCPDS No. 98-001-1687) with space group p $\bar{3}m$  [35]. The absence of the diffraction peaks of CuO or Cu discloses that Cu<sub>2</sub>O grew in its pure phase. The more intense diffraction peaks insinuate that the obtained Cu<sub>2</sub>O nano hexapods have a high degree of crystallinity. The XRD patterns of the hybrid heterostructures vividly exhibit the characteristic peaks of both the ZIS and Cu<sub>2</sub>O. Besides, the intensity of (006), (108), (110) and (022) planes decreased with increasing Cu<sub>2</sub>O amount from 5 to 20 wt%, suggesting the formation of heterostructure between ZIS and Cu<sub>2</sub>O. On the contrary, no change in the peak positions of the heterostructure was found, revealing that the crystal structure of either compound is unaffected. The crystallite size of as-synthesized

compositions was estimated by the Debye-Scherrer formula.

$$t = \frac{0.9\lambda}{\beta \cos \theta} \quad (1)$$

where “ $t$ ” is the average crystallite size, “ $\lambda$ ” is X-rays wavelength (1.5406 Å), “ $\beta$ ” is fullwidth at half maximum (FWHM) of the highest intensity peak (in radians), “ $\theta$ ” is the Bragg’s angle of the crystal planes. The dislocation density of the pure components and their composites were calculated by the following formula.

$$\text{Dislocation density } (\delta) = \frac{1}{(\text{Crystalline size})^2} \quad (2)$$

The strain of the materials was calculated by the following equation.

$$\text{Strain } (\epsilon) = \frac{\beta \cos \theta}{4} \quad (3)$$

The crystallite size ( $t$ ), dislocation density ( $\delta$ ) and strain ( $\epsilon$ ) of all the compounds are listed in Table 1. The unit cells of both Cu<sub>2</sub>O and ZIS were drawn with VESTA software and presented in Fig. 2(b).

#### 3.2. Raman spectroscopy

Fig. 3. displays the Raman spectra of pure ZIS, Cu<sub>2</sub>O and ZIS-10 composites in the wave number range of 100–800 cm<sup>−1</sup>. The pure ZIS exhibits two prominent characteristic Raman bands at 241 and 352 cm<sup>−1</sup>. The band observed at 241 (A<sub>1g</sub>) cm<sup>−1</sup> is due to the molecular vibration of M-S (M = Zn, In) and the band at 352 cm<sup>−1</sup> is corresponding to the symmetric stretching of S-S bonds in the octahedral structure [6,45]. Similarly, the appearance of five bands at 113, 150, 217, 408 and 625 cm<sup>−1</sup> in the Raman spectrum of Cu<sub>2</sub>O confirms the single phase and is well corroborated with the reported literature [46]. The peaks at 113 and 150 cm<sup>−1</sup> are assigned to Raman inactive and scattering modes from phonons of symmetry  $\Gamma_{15}^-$  respectively [46]. The high intense Raman band observed at 217 cm<sup>−1</sup> is attributed to the second-order Raman-allowed mode as well as the overtone mode of Cu<sub>2</sub>O [47]. The less intense band at 408 cm<sup>−1</sup> and moderately intense band at 625 cm<sup>−1</sup> are linked to four phonons of  $3\Gamma_{12}^- + \Gamma_{25}^-$  and infrared-allowed mode respectively [48,49]. It can be seen from Fig. 3, the Raman bands of ZIS-10 are found to be blue-shifted while their intensity remarkably changed. It clearly suggests that the negatively charged oxygen atoms of Cu<sub>2</sub>O electrostatically interact with the negatively charged sulfur atoms of ZIS at the interfacial surface, thereby affecting the bond distance between Zn-S/S-In. Thus, the appeared blue shift demonstrates the formation of heterostructure between the ZIS and Cu<sub>2</sub>O nanostructures.

#### 3.3. UV-Vis DRS analysis

The optical properties of synthesized materials were determined by UV-Vis DRS and the resultant spectra of pure ZIS, Cu<sub>2</sub>O and composites are shown in Fig. 4(a), demonstrating that pure ZIS and Cu<sub>2</sub>O have a sharp absorption edge around 520 and 640 nm, respectively. The absorption edges of ZIS-5, ZIS-10 and ZIS-20 nanocomposites manifested a redshift. The optical band gap ( $E_g$ ) of materials is calculated using the relation.

$$\alpha h\nu = A (h\nu - E_g)^{1/2} \quad (4)$$

where  $A$  is a constant.

The obtained  $E_g$  values from a Tauc plot (Fig. 4(b)) of ZIS, Cu<sub>2</sub>O, ZIS-5, ZIS-10 and ZIS-20, respectively are 2.46, 2.01, 2.36, 2.24 and 2.16 eV. As displayed in Fig. 4(b), ZIS has a higher optical band gap than Cu<sub>2</sub>O. Besides, Cu<sub>2</sub>O exhibited a broad absorption range, whereas ZIS has a narrow absorption range. In addition, the heterostructures showed less absorbance than pure compounds, resulting from more scattering of light by the heterostructure wherein Cu<sub>2</sub>O agglomerated over ZIS or vice versa, leading to suppression of the light absorption. This result

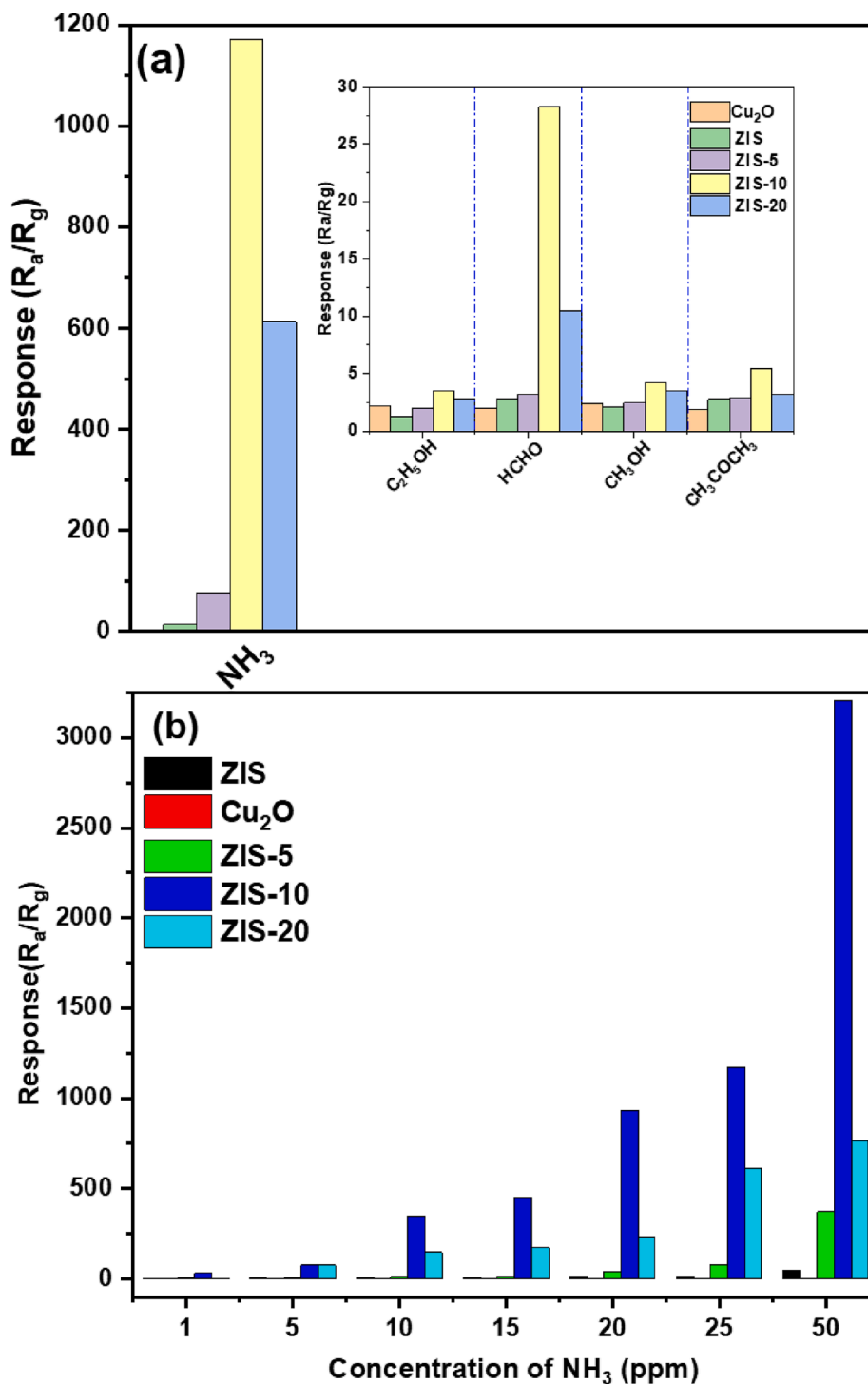


Fig. 8. (a) Selectivity and (b) response ( $R_a/R_g$ ) Vs concentration of NH<sub>3</sub> gas in the presence of all the compositions.

validates the SEM and TEM analysis. The top of valence band (VB) of Cu<sub>2</sub>O contains Cu 3d and O 2p as main orbitals where Cu 3d contributes to the top of VB and O 2p at the bottom of VB and the bottom of conduction band (CB) might composed of anti-bonding Cu 4p + Cu 3d and O 2p orbitals [50]. On the other hand, VB of ZIS is majorly made of S 3p + In 5p + Zn 3d + Zn 4p and its CB contributed by Zn 4s + S 3p + In 5s + In 5p of CB of ZIS [51]. The random variation in the optical band gap is attributed to the possible interaction between ZnIn<sub>2</sub>S<sub>4</sub> and Cu<sub>2</sub>O. At the interface of the heterostructure, the S ions electrostatically interact with O ions (see Fig. 2 (b)), leading to the repulsion between the 3p electrons of S ions and the 2p electrons of O ions. Consequently, this interaction

would affect the bond lengths of O-Cu and S-Zn or S-In. This indeed significantly modifies the electronic band structure of both the VB and CB of the respective compounds. Thus, this could be accountable for the observed variation in the optical band gap.

### 3.4. XPS analysis

To determine the valence states of the elements, present in the ZIS-10 nanocomposite XPS was used. The survey spectrum of ZIS-10 heterostructure (Fig. 5(a)) shows sharp peaks, suggesting the presence of only Zn, In, S, Cu and O elements. The two prominent peaks centered at

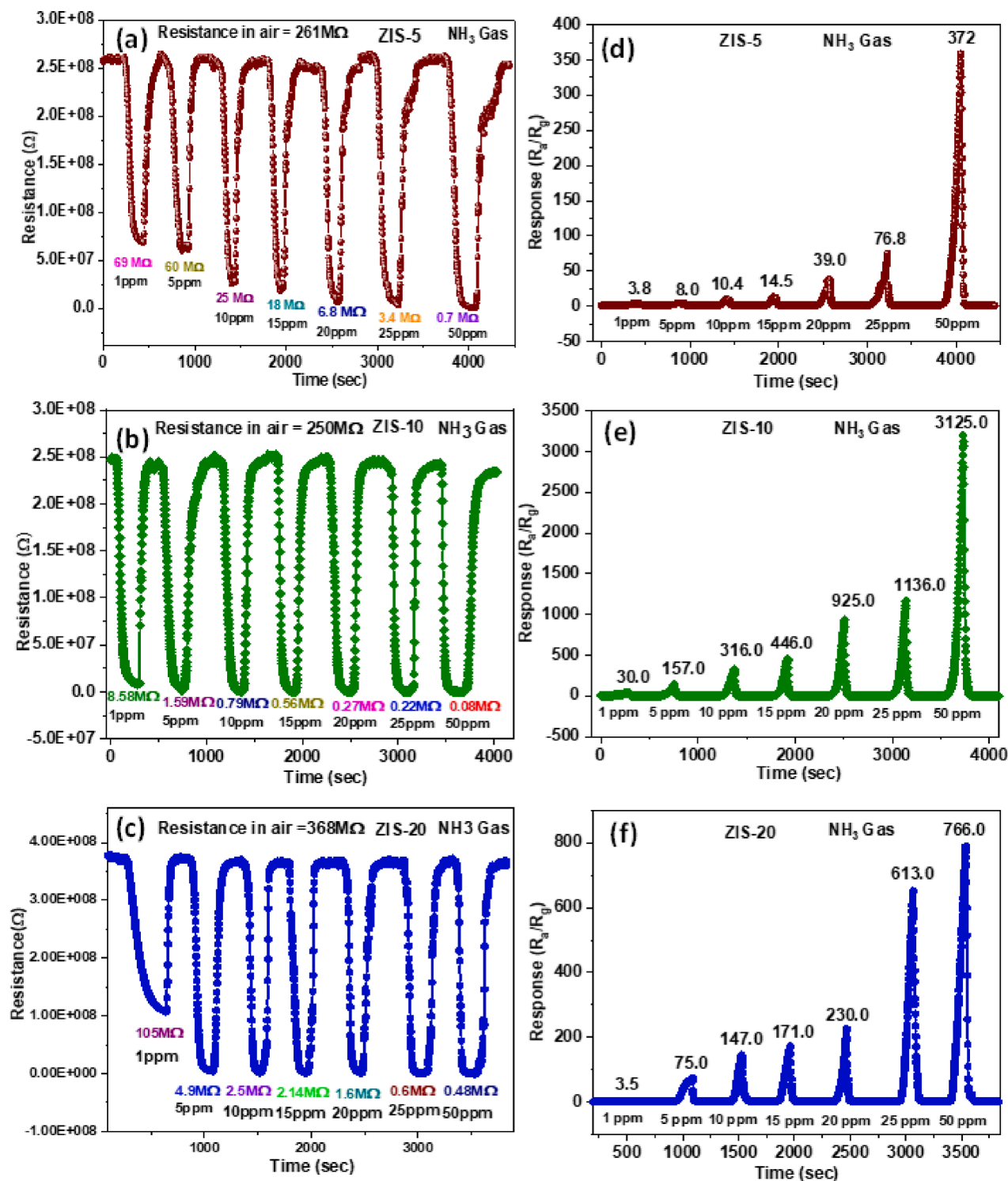


Fig. 9. Dynamic response of (a, d) ZIS-5, (b, e) ZIS-10 and (c, f) ZIS-20.

1022.96 and 1046.13 eV (Fig. 5(b)) attributed to Zn 2p<sub>3/2</sub> and Zn 2p<sub>1/2</sub> respectively, assured that Zn exists in the +2 state [52]. As disclosed in Fig. 5(c) the two major peaks seen at 445.8 (3d<sub>5/2</sub>) and 453.5 (3d<sub>3/2</sub>) eV are ascertained to be +3 oxidation state of In. The XPS spectrum of S was fitted into two sub peaks using the Gaussian function and shown in Fig. 5(d). The two peaks observed at 161.9 and 163.4 eV, corresponding to S 2p<sub>3/2</sub> and S 2p<sub>1/2</sub> respectively, indicate that S is present in the -2 oxidation state (S<sup>2-</sup>) [52]. In addition, Cu 2p has the two characteristic peaks, observed at 932.8 and 952.6 eV along with the satellite peaks at a

lower binding energy of 934.7 and 954.7 eV, respectively, corresponding to Cu 2p<sub>3/2</sub> and Cu 2p<sub>1/2</sub> indicating Cu<sup>+</sup> state (Fig. 5(e)) [53]. This observation strongly advocates the XRD results of Cu<sub>2</sub>O. The high-resolution spectrum of O 1s displayed an intense peak at 532.5 eV as shown in Fig. 5(f), assigned to lattice oxygens with Cu-O bonds. In short, it is strongly believed from XPS analysis carried out on ZIS-10 heterostructure that the compounds formed in their respective single phases.

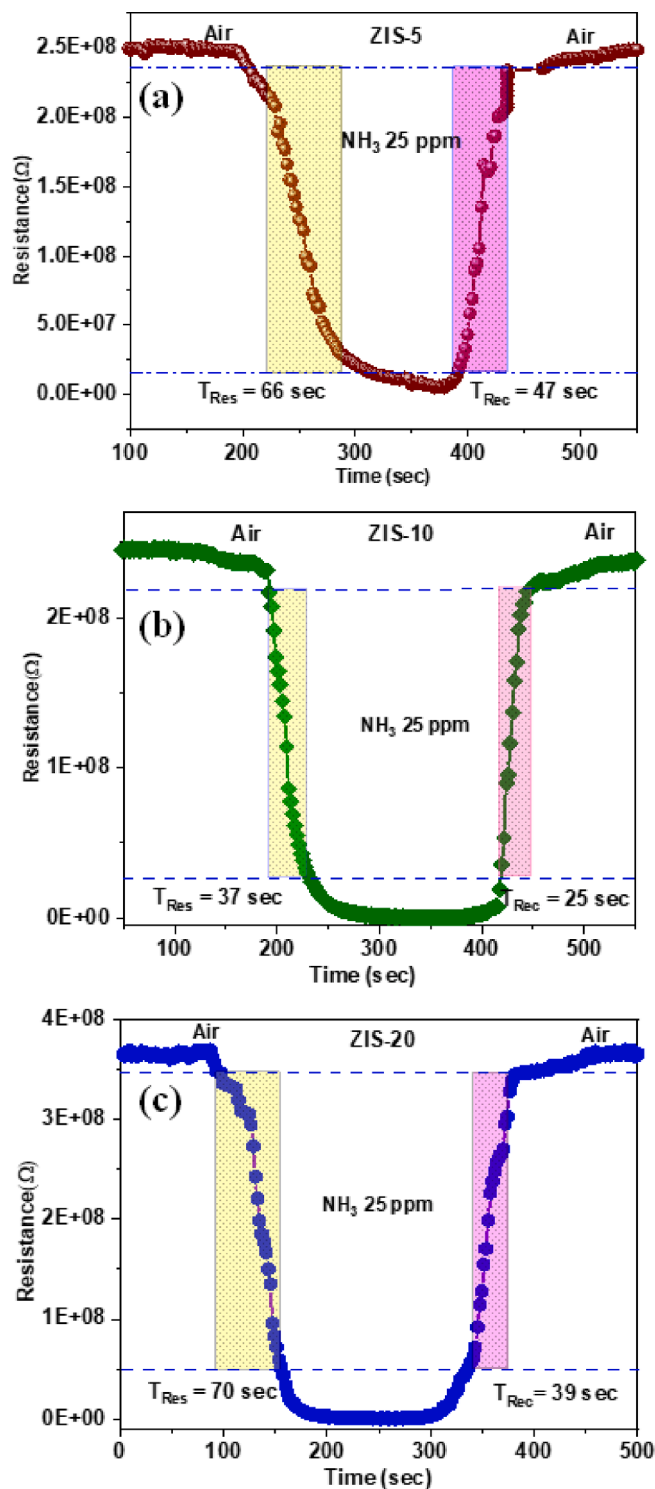


Fig. 10. Response/recovery time of (a) ZIS-5, (b) ZIS-10 and (c) ZIS-20.

### 3.5. SEM and HRTEM analysis

The morphology and nanostructure of the materials were examined by SEM and HRTEM. Fig. 6(a-c) shows the SEM images of all the compounds with different magnifications. As illustrated in Fig. 6(a), pure ZIS primarily made of a flower-like hierarchical structure with an average diameter of 2–3  $\mu\text{m}$  and it has several layers of petaloid structures, endowing this material to possess mesoporous and microporous features. The  $\text{Cu}_2\text{O}$  compound majorly consists of microcrystals as shown in Fig. 6(b), which have hexapod morphology with an average size

Table 2

Response and the recovery time of different sensors towards ammonia ( $\text{NH}_3$ ) at room temperature.

Compound	Preparation method	Concentration (ppm)	Response	$T_{\text{res}}/T_{\text{rec}}$ (sec)	Ref.
$\text{SnO}_2$	Sol-gel	50	694	175/210	[59]
Ce doped $\text{SnO}_2$	Hydrothermal	25	11	60/35	[60]
$\text{TiO}_2$	Sol-gel	50	35	240/360	[61]
$\text{In}_2\text{O}_3$	Thermal Oxidation	1000	92	100/60	[62]
Co-doped ZnO	Spray pyrolysis	100	3.48	36/10	[63]
PPy/ $\text{Zn}_2\text{SnO}_4$	Hydrothermal	100	82.1	26/24	[64]
$\text{CuO-MnO}_2$	Hydrothermal	100	135	120/600	[65]
Mn-doped ZnO	Combustion	100	20.2	73/147	[66]
NiO/ZnO	Hydrothermal	50	42	27/150	[67]
$\text{ZnIn}_2\text{S}_4/\text{Cu}_2\text{O}$	Hydrothermal	25	37/25		Present work

between 1 and 3  $\mu\text{m}$  and are congruent with the previous report [54]. The addition of  $\text{Cu}_2\text{O}$  from 5 to 20 wt% to ZIS did not significantly alter the morphology of the resultant heterostructure. However, from Fig. 6 (c), it is evident that the high agglomeration of heterostructure resulted from the random distribution of  $\text{Cu}_2\text{O}$  microcrystals embellished over the ZIS micro flower, leading to the formation of an interface between ZIS and  $\text{Cu}_2\text{O}$ . The presence of  $\text{Cu}_2\text{O}$  and ZIS is further asserted by EDX analysis. The EDS elemental mapping images are shown in Fig. 6(d), displaying that Zn, In, S, Cu, and O are evenly dispersed throughout the ZIS-10 composite. The HRTEM images of ZIS-10 (Fig. 6(e)) exhibit the microstructure which consists of nanosheet-like structures and nanoparticles. The interplanar spacing was (Fig. 6(f)) found to be 0.317 nm and 0.20 nm corresponding to the (012) and (110) planes respectively of ZIS and the lattice spacing of 0.15 nm is ascribed to the (022) plane of  $\text{Cu}_2\text{O}$ . The SAED pattern of ZIS-10 (Fig. 6(g)) indicates the high crystallinity of the sample and is corroborated by the XRD results.

### 3.6. BET surface area analysis

To determine the BET surface area of ZIS,  $\text{Cu}_2\text{O}$  and ZIS-10 materials,  $\text{N}_2$  adsorption studies were conducted, and the results are presented in Fig. 7. The presence of a significant type IV hysteresis loop observed within the relative pressure range from 0.5 to 0.9 provides evidence for the mesoporous nature of the ZIS and ZIS-10 materials. However,  $\text{Cu}_2\text{O}$  exhibits a narrow loop, indicating its microporous nature. As the  $\text{Cu}_2\text{O}$  amount increases from 5 to 20 wt%, the width of the hysteresis loop decreases, implying the dominance of the microporous nature of the material over its mesoporous nature. The results obtained from the BET analysis revealed that the surface areas of ZIS,  $\text{Cu}_2\text{O}$  and ZIS-10 are 25.84, 0.66 and 13.23  $\text{m}^2/\text{g}$ , respectively. The large surface area is due to the hierarchical structures of the ZIS materials whereas the decrease in the surface area of ZIS-10 is due to the dispersion of the hexapods of  $\text{Cu}_2\text{O}$  over the ZIS micro-flowers with high agglomeration which was further substantiated by SEM results. Volanti et al. [31] have also noticed similar results and confirmed that factors other than surface area are responsible for the enhanced sensor's response.

### 3.7. Gas sensing properties

The selectivity, sensitivity and response ( $S = R_a/R_g$ ) of ZIS,  $\text{Cu}_2\text{O}$  and all the composites towards different volatile organic compounds (VOCs)

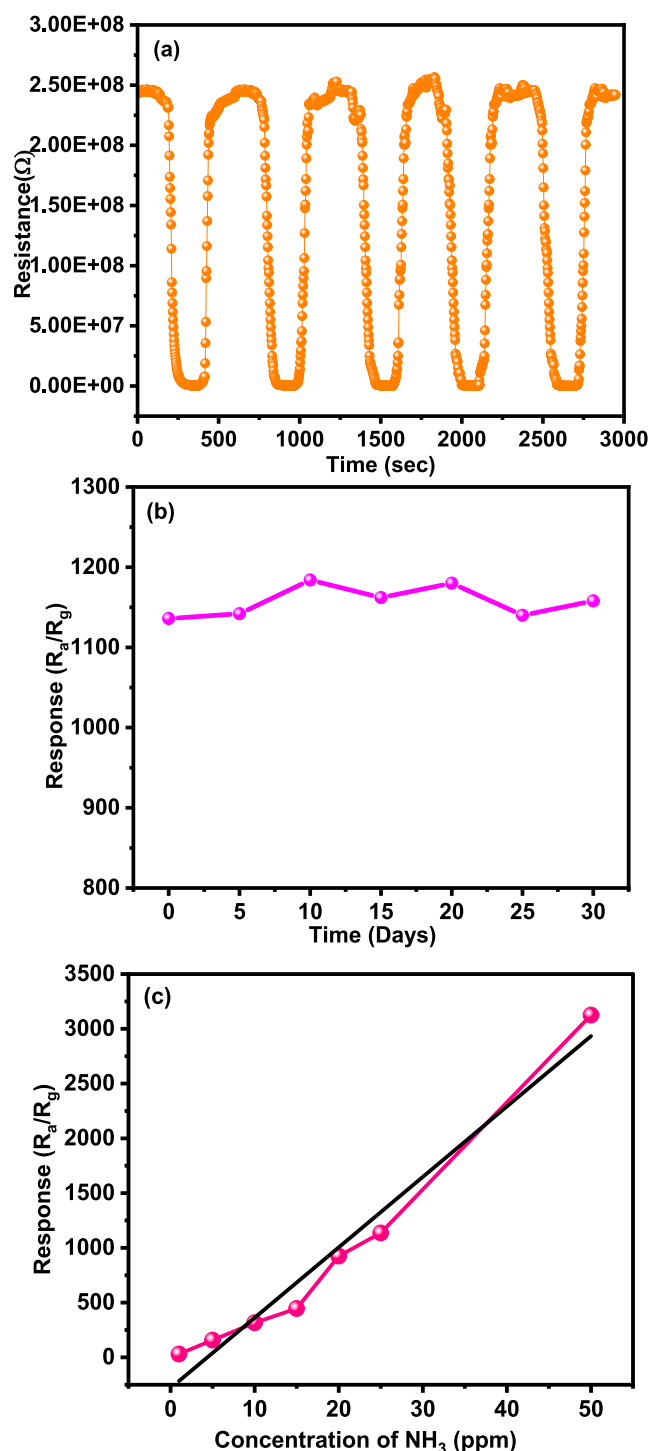


Fig. 11. (a) Repeatability and (b) stability of ZIS-10 towards 25 ppm ammonia gas at RT and (c) Response variation of ZIS-10 towards different  $\text{NH}_3$  concentration (LOD).

were determined by measuring  $R_c$ . In this study, formaldehyde, ethyl alcohol, benzene, toluene and xylene were chosen as VOC's. However, the response of the semiconductors is a function of the operating temperature, concentration (ppm) and kinetic diameter of the gas. Thus, initially, the selectivity of all compounds was tested with 25 ppm of the above VOCs. Fig. 8(a) displays the response of  $\text{NH}_3$  whereas the inset shows the response of the rest of the gases since  $\text{NH}_3$  response-masked the other gases. The highest response towards  $\text{NH}_3$  gas is owing to its lower kinetic diameter (260 pico meter) than other gases. Thereby,  $\text{NH}_3$

molecules easily diffuse onto the sensing material's surface. It is worth noting that all the compositions exhibited gas-sensing properties at RT, which is essential for its practical applications. Therefore, the concentration-dependent measurements for all the samples were carried out with  $\text{NH}_3$  at RT only. The response of all the materials towards ammonia at various concentrations (1, 5, 10, 15, 20 and 50 ppm) is shown in Fig. 8(b). The dynamic response and recovery of pure ZIS and  $\text{Cu}_2\text{O}$  are shown in Fig. S2 (a-d). The dynamic response of ZIS,  $\text{Cu}_2\text{O}$  and the composites (Fig. 9) profoundly increases with the increase of  $\text{NH}_3$  concentration. It should be noted that ZIS-10 has manifested the highest response among all the other samples. For 25 ppm, the response (S) of ZIS,  $\text{Cu}_2\text{O}$ , ZIS-5, ZIS-10 and ZIS-20 are respectively, measured to be 15, 2.5, 75, 1167 and 652, proving that ZIS-10 has astronomical response i. e., 476 and 81 times higher than of the pristine  $\text{Cu}_2\text{O}$  and ZIS, respectively.

### 3.8. Response and recovery characteristics

The response time ( $T_{\text{res}}$ ) of the sensor is defined as the time during which the sensor's resistance reduces to 90% of its saturation resistance in the presence of gas. Likewise, the recovery time ( $T_{\text{rec}}$ ) is the time needed by a sensor to return to 10% saturated resistance after the withdrawal of gas. The values of response time and recovery time of all the composites were computed from Fig. 10. The response/recovery ( $T_{\text{res}}/T_{\text{rec}}$ ) times of ZIS,  $\text{Cu}_2\text{O}$  (Fig. S3 (a, b)), ZIS-5, ZIS-10 and ZIS-20 were determined in the presence of 25 ppm of  $\text{NH}_3$ , and found to be 98/88, 117/50, 66/47, 37/25 and 70/39, respectively. It indicates that ZIS-10 has shorter  $T_{\text{res}}/T_{\text{rec}}$  than all the other compounds. Table 2 compares various sensors' responses and recovery time towards  $\text{NH}_3$  gas at RT. The high repeatability and stability of gas-sensing materials accentuate the applicability of these materials for their real-time applications. Thus, the repeatability and stability of highly responsive ZIS-10 were investigated for 25 ppm of  $\text{NH}_3$  over five cycles (Fig. 11(a)) and the observed results, conclusively reflect that ZIS-10 has applause repeatability towards  $\text{NH}_3$  at RT. Apart from this, the stability (Fig. 11 (b)) was tested over 30 days with an interval of 5 days and the observations not only demonstrated the stability of ZIS-10 at each interval but also showed its remarkable stability over 30 days. The limit of detection (Fig. 11(c)) was determined using the following equation and found to be 14.9 ppm.

$$\text{Limit of Detection (LOD)} = 3.0 \times \frac{\text{Standard Deviation (SD)}}{\text{Slope of the Curve}} \quad (5)$$

### 3.9. Gas sensing mechanism

The basic gas sensing mechanism involves the physicochemical interaction between the analyte gas molecules and the surface of the sensor [31]. The formation of p-n heterojunction is shown in Fig. 12(a) and the gas sensing mechanism for highly responsive ZIS-10 is proposed. Initially,  $\text{O}_2$  molecules adsorbed on the ZIS-10 surface, consequently, these adsorbed  $\text{O}_2$  simultaneously grab the electrons primarily from S 3p + In 5s + Cu 3d + O 2p of CB of ZIS-10, thereby forming umpteen oxygen ions ( $\text{O}_2^-$ ) at RT [55]. Hence, the electron cloud at the surface decreases, as a result, the depletion layer is formed, leading to an increase in the resistance of ZIS-10. Thereafter, ZIS-10 in the presence of  $\text{NH}_3$  vapors, the strong interaction between the chemisorbed  $\text{O}_2^-$  and  $\text{NH}_3$  molecules releases abundant electrons and readily injects into the CB of ZIS-10. Thus, the thickness of the depletion layer decreases, leading to decrease in resistance of ZIS-10. Furthermore, the under-mentioned factors also contribute to decreasing the resistance. The electron affinity ( $\chi$ ) of  $\text{Cu}_2\text{O}$  and ZIS are 5.32 and 4.86 eV, respectively [56,57]. The difference between  $\chi$  of these two compounds alongside their effective energy band gap, which might vary their work functions and conduction and valence band offsets. Thereby these features facilitate the electrons to transfer from S 3p + In 5s of CB of ZIS to primarily



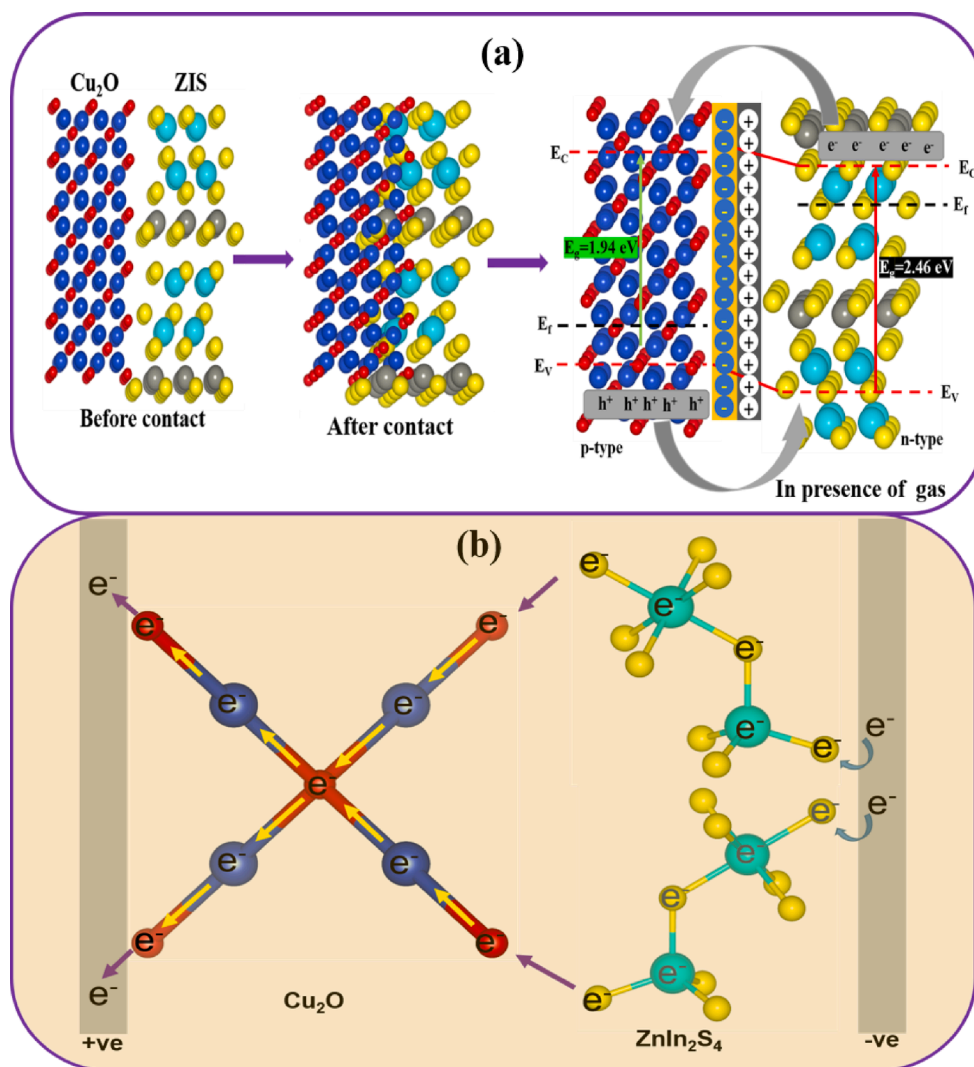
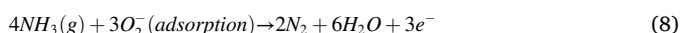
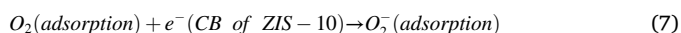
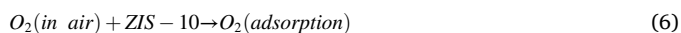


Fig. 12. (a) Energy band diagram of p-Cu<sub>2</sub>O/n-ZnIn<sub>2</sub>S<sub>4</sub> heterostructure (b) schematic representation of gas sensing mechanism.

Cu 3d + O 2p of CB of Cu<sub>2</sub>O at the intimate interface of ZIS-10 heterostructure. More clearly, at the p-n heterojunction interface, it is conceived that the electrons easily migrate from ZIS to Cu<sub>2</sub>O through the conducting channel viz., -S-In-S-In-S-O-Cu-O- as schematically depicted in Fig. 12(b). This channel might offer a low resistance path for the electrons between the contact electrodes. Having said that, the other possible pathway such as -S-Zn-S-Zn-S-O-Cu-O- might provide high resistance channel for the electrons since Zn 4s and Zn 4p orbitals contribute to the top of CB of ZIS-10 than that of In and S orbitals [58]. Alternately, since Cu<sup>+</sup> ions coordinated by their nearest neighbor 12 Cu<sup>+</sup> ions resulted in the moderate Cu-Cu interaction thereby various d-d orbitals of Cu<sup>+</sup> - Cu<sup>+</sup> undergo hybridization up to the possible extent, creating the other conducting paths for itinerant electrons. Thus, electrons also find the other pathways from Cu<sup>+</sup> to neighboring Cu<sup>+</sup> ions in addition to -S-In-S-In-S-O-Cu-O-. These additional pathways partly cause ZIS-10 to possess a lower resistance than other compounds. All in all, these peculiar pathways are more responsible for ZIS-10 to have an enormous response towards low ppm detection of NH<sub>3</sub> gas.

The underlying mechanism is as follows.



#### 4. Conclusions

In summary, we have successfully synthesized ZnIn<sub>2</sub>S<sub>4</sub>/Cu<sub>2</sub>O heterostructures that exhibit a highly sensitive and rapidly responsive ammonia gas sensor, while maintaining remarkable stability. Among all the composites tested, ZIS-10 exhibits outstanding performance in ammonia sensing at RT, detecting concentrations as low as 1 ppm. The responses of ZIS-10 measured to be 1184 which is 81 and 476 times higher compared to the pristine ZIS and Cu<sub>2</sub>O, respectively. Additionally, ZIS-10 exhibited shorter response and recovery times ( $T_{\text{res}}/T_{\text{rec}}$ ) compared to other compounds, with values of 37/25. The enhanced sensing capabilities of ZIS-10 can be attributed to the difference in electron affinities ( $\chi$ ) between the two compounds. This difference facilitates the transfer of electrons from the CB of ZIS especially from S 3p + In 5s, to the Cu 3d + O 2p of CB of Cu<sub>2</sub>O at the interface of ZIS-10 heterostructure. Furthermore, electrons find the alternative pathways from Cu<sup>+</sup> to neighboring Cu<sup>+</sup> ions, in addition to the -S-In-S-In-S-O-Cu-O- pathway. These additional pathways contribute to ZIS-10 having low resistance compared to other compounds.

#### CRediT authorship contribution statement

**Kranthi Kumar Bedala:** Methodology, Formal analysis, Data curation, Writing – original draft. **Prasad Gonugunta:** Investigation,

Writing – review & editing. **Eszter Mádaí:** Investigation. **Peyman Taheri:** Resources, Writing – review & editing. **Sandeep Kumar Padamati:** Writing – review & editing. **P. Nagaraju:** Writing – review & editing. **G. Upender:** Writing – review & editing. **B. Vijaya Kumar:** Conceptualization, Investigation, Supervision, Project administration, Writing – review & editing.

## Declaration of Competing Interest

The authors declare that they have no known competing financial interests or personal relationships that could have appeared to influence the work reported in this paper.

## Data availability

Data will be made available on request.

## Appendix A. Supplementary data

Supplementary data to this article can be found online at <https://doi.org/10.1016/j.apsusc.2023.158315>.

## References

- [1] R.J. Willey, West Fertilizer Company fire and explosion: A summary of the US Chemical Safety and Hazard Investigation Board report, *J. Loss Prev. Process Ind.* 49 (2017) 132–138.
- [2] M. Punginsang, D. Zappa, E. Comini, A. Wisitsoraat, G. Sberveglieri, A. Ponzoni, C. Liewhiran, Selective H<sub>2</sub>S gas sensors based on ohmic hetero-interface of Au-functionalized WO<sub>3</sub> nanowires, *Appl. Surf. Sci.* 571 (2022), 151262.
- [3] F. Qin, J. Gao, L. Jiang, J. Fan, B. Sun, Y. Fan, H. Lv, K. Shi, Biomimetic WO<sub>3</sub>@WS<sub>2</sub> heterojunction composites for enhanced NO<sub>2</sub> gas-sensing performance at room temperature, *Appl. Surf. Sci.* 615 (2023), 156338.
- [4] Z. Zhang, Z. Wen, Z. Ye, L. Zhu, Ultrasensitive ppb-level NO<sub>2</sub> gas sensor based on WO<sub>3</sub> hollow nanospheres doped with Fe, *Appl. Surf. Sci.* 434 (2018) 891–897.
- [5] H. Gao, L. Zhu, X. Peng, X. Zhou, M. Qiu, Fe-doped WO<sub>3</sub> nanoplates with excellent bifunctional performances: Gas sensing and visible light photocatalytic degradation, *Appl. Surf. Sci.* 592 (2022), 153310.
- [6] C. Dong, R. Zhao, L. Yao, Y. Ran, X. Zhang, Y. Wang, A review on WO<sub>3</sub> based gas sensors: Morphology control and enhanced sensing properties, *J. Alloys Compd.* 820 (2020), 153194.
- [7] Y. Qiu, Y. Wang, Synthesis, growth kinetics and ultra-sensitive performance of electropun WO<sub>3</sub> nanofibers for NO<sub>2</sub> detection, *Appl. Surf. Sci.* 608 (2023), 155112.
- [8] X. Liu, L. Jiang, X. Jiang, X. Tian, X. Sun, Y. Wang, W. He, P. Hou, X. Deng, X. Xu, Synthesis of Ce-doped In<sub>2</sub>O<sub>3</sub> nanostructure for gas sensor applications, *Appl. Surf. Sci.* 428 (2018) 478–484.
- [9] D. Li, Y. Li, X. Wang, G. Sun, J. Cao, Y. Wang, Surface modification of In<sub>2</sub>O<sub>3</sub> porous nanospheres with Au single atoms for ultrafast and highly sensitive detection of CO, *Appl. Surf. Sci.* 613 (2023), 155987.
- [10] E. Cao, L. Wu, Y. Zhang, L. Sun, Z. Yu, Z. Nie, Hydrothermal synthesis of cubic-rhombohedral-In<sub>2</sub>O<sub>3</sub> microspheres with superior acetone sensing performance, *Appl. Surf. Sci.* 613 (2023), 156045.
- [11] D. Wang, C. Han, C. Zheng, H. Fang, D. Xu, H. Zhao, Fabrication of a ppb-level NO<sub>2</sub> gas sensor by sensitizing nanobundles assembled by In<sub>2</sub>O<sub>3</sub> nanotubes with TiO<sub>2</sub> quantum dots, *Sens. Actuators B Chem.* 387 (2023), 133833.
- [12] Y. Bai, H. Fu, X. Yang, S. Xiong, S. Li, X. An, Conductometric isopropanol gas sensor: Ce-doped In<sub>2</sub>O<sub>3</sub> nanosheet-assembled hierarchical microstructure, *Sens. Actuators B Chem.* 377 (2023), 133007.
- [13] J. Hu, X. Wang, M. Zhang, Y. Sun, P. Li, W. Zhang, K. Lian, L. Chen, Y. Chen, Synthesis and characterization of flower-like MoO<sub>3</sub>/In<sub>2</sub>O<sub>3</sub> microstructures for highly sensitive ethanol detection, *RSC Adv.* 7 (2017) 23478–23485.
- [14] X. Ma, H. Zhu, L. Yu, X. Li, E. Ye, Z. Li, X.J. Loh, S. Wang, Rare-earth-doped indium oxide nanosphere-based gas sensor for highly sensitive formaldehyde detection at a low temperature, *Nanoscale* 15 (2023) 1609–1618.
- [15] H. Fu, X. Yang, Z. Wu, P. He, S. Xiong, D. Han, X. An, Gas-sensing performance of In<sub>2</sub>O<sub>3</sub>@MoO<sub>3</sub> hollow core-shell nanospheres prepared by a two-step hydrothermal method, *Sens. Actuators B Chem.* 352 (2022), 131007.
- [16] A. Sharma, M. Tomar, V. Gupta, Room temperature trace level detection of NO<sub>2</sub> gas using SnO<sub>2</sub> modified carbon nanotubes based sensor, *J. Mater. Chem.* 22 (2012) 23608–23616.
- [17] L. Zhou, Z. Hu, P. Wang, N. Gao, B. Zhai, M. Ouyang, G. Zhang, B. Chen, J. Luo, S. Jiang, H.-Y. Li, H. Liu, Enhanced NO<sub>2</sub> sensitivity of SnO<sub>2</sub> SAW gas sensors by facet engineering, *Sens. Actuators B Chem.* 361 (2022), 131735.
- [18] M. Inaba, T. Oda, M. Kono, N. Phansiri, T. Morita, S. Nakahara, M. Nakano, J. Suehiro, Effect of mixing ratio on NO<sub>2</sub> gas sensor response with SnO<sub>2</sub>-decorated carbon nanotube channels fabricated by one-step dielectrophoretic assembly, *Sens. Actuators B Chem.* 344 (2021), 130257.
- [19] B. Li, Q. Zhou, S. Peng, Y. Liao, Recent advances of SnO<sub>2</sub>-based sensors for detecting volatile organic compounds, *Fron. Chem.* 8 (2020) 321.
- [20] Q. Wan, Q. Li, Y. Chen, T.-H. Wang, X. He, J. Li, C. Lin, Fabrication and ethanol sensing characteristics of ZnO nanowire gas sensors, *App. Phys. Lett.* 84 (2004) 3654–3656.
- [21] H. Xu, X. Liu, D. Cui, M. Li, M. Jiang, A novel method for improving the performance of ZnO gas sensors, *Sens. Actuators B Chem.* 114 (2006) 301–307.
- [22] Y. Kang, F. Yu, L. Zhang, W. Wang, L. Chen, Y. Li, Review of ZnO-based nanomaterials in gas sensors, *Solid State Ion.* 360 (2021), 115544.
- [23] Z. Li, Z. Yao, A.A. Haidry, T. Plecenik, L. Xie, L. Sun, Q. Fatima, Resistive-type hydrogen gas sensor based on TiO<sub>2</sub>: A review, *Int. J. Hydrog. Energy* 43 (2018) 21114–21132.
- [24] M. Ferroni, V. Guidi, G. Martinelli, G. Faglia, P. Nelli, G. Sberveglieri, Characterization of a nanosized TiO<sub>2</sub> gas sensor, *Nanostruct. Mater.* 7 (1996) 709–718.
- [25] D. Xue, R. Zhou, X. Lin, X. Duan, Q. Li, T. Wang, A highly selective and sensitive H<sub>2</sub>S sensor at low temperatures based on Cr-doped  $\alpha$ -Fe<sub>2</sub>O<sub>3</sub> nanoparticles, *RSC Adv.* 9 (2019) 4150–4156.
- [26] L. Yin, D. Chen, M. Feng, L. Ge, D. Yang, Z. Song, B. Fan, R. Zhang, G. Shao, Hierarchical Fe<sub>2</sub>O<sub>3</sub>@WO<sub>3</sub> nanostructures with ultrahigh specific surface areas: microwave-assisted synthesis and enhanced H<sub>2</sub>S-sensing performance, *RSC Adv.* 5 (2015) 328–337.
- [27] S. Kumar, A. Singh, R. Singh, S. Singh, P. Kumar, R. Kumar, Facile h-MoO<sub>3</sub> synthesis for NH<sub>3</sub> gas sensing application at moderate operating temperature, *Sens. Actuators B Chem.* 325 (2020), 128974.
- [28] S. Ananthi, M. Kavitha, A. Balamurugan, E.R. Kumar, G. Magesh, A.F. Abd El-Rehim, C. Srinivas, P. Anilkumar, J. Suryakanth, C.S. Rahale, Synthesis, analysis and characterization of camellia sinensis mediated synthesis of NiO nanoparticles for ethanol gas sensor applications, *Sens. Actuators B Chem.* 387 (2023), 133742.
- [29] C. Li, P.G. Choi, K. Kim, Y. Masuda, High-performance acetone gas sensor based on ultrathin porous NiO nanosheet, *Sens. Actuators B Chem.* 367 (2022), 132143.
- [30] P. Li, C. Cao, Q. Shen, B. Bai, H. Jin, J. Yu, W. Chen, W. Song, Cr-doped NiO nanoparticles as selective and stable gas sensor for ppb-level detection of benzyl mercaptan, *Sens. Actuators B Chem.* 339 (2021), 129886.
- [31] D.P. Volanti, A.A. Felix, M.O. Orlandi, G. Whitfield, D.J. Yang, E. Longo, H. L. Tuller, J.A. Varela, The role of hierarchical morphologies in the superior gas sensing performance of CuO-based chemiresistors, *Adv. Funct. Mater.* 23 (2013) 1759–1766.
- [32] T. Hemalatha, S. Akilandeswari, T. Krishnakumar, S.G. Leonardi, G. Neri, N. Donato, Comparison of electrical and sensing properties of pure, Sn- and Zn-doped CuO gas sensors, *IEEE Trans. Instrum. Meas.* 68 (2018) 903–912.
- [33] K. Zhao, X. Li, J. Tang, H. Yang, Q. Wu, X. Wang, X. Guo, D. Zeng, Effect of exposed facet determined the room-temperature ammonia gas sensing of Cu<sub>2</sub>O nanoparticles, *Appl. Surf. Sci.* 613 (2023), 156008.
- [34] J. Hu, C. Zou, Y. Su, M. Li, Y. Han, E.-S.-W. Kong, Z. Yang, Y. Zhang, An ultrasensitive NO<sub>2</sub> gas sensor based on a hierarchical Cu<sub>2</sub>O/CuO mesocrystal nanoflower, *J. Mater. Chem. A* 6 (2018) 17120–17131.
- [35] X. Wan, J. Wang, L. Zhu, J. Tang, Gas sensing properties of Cu<sub>2</sub>O and its particle size and morphology-dependent gas-detection sensitivity, *J. Mater. Chem. A* 2 (2014) 13641–13647.
- [36] S. Deng, V. Tjoa, H.M. Fan, H.R. Tan, D.C. Sayle, M. Olivo, S. Mhaisalkar, J. Wei, C. H. Sow, Reduced graphene oxide conjugated Cu<sub>2</sub>O nanowire mesocrystals for high-performance NO<sub>2</sub> gas sensor, *J. Am. Chem. Soc.* 134 (2012) 4905–4917.
- [37] H. Sun, M. Cao, P. Zhang, X. Tian, M. Lu, L. Du, K. Xue, G. Cui, Magnetic-field-enhanced H<sub>2</sub>S sensitivity of Cu<sub>2</sub>O/NiO heterostructure ordered nanoarrays, *ACS Sens.* 7 (2022) 1903–1911.
- [38] Y. Ding, X. Guo, B. Du, X. Hu, X. Yang, Y. He, Y. Zhou, Z. Zang, Low-operating temperature ammonia sensor based on Cu<sub>2</sub>O nanoparticles decorated with p-type MoS<sub>2</sub> nanosheets, *J. Mater. Chem. C* 9 (2021) 4838–4846.
- [39] R.R. Kumar, W.C. Yu, T. Murugesan, P.C. Chen, A. Ranjan, M.Y. Lu, H.N. Lin, Formation of large-scale MoS<sub>2</sub>/Cu<sub>2</sub>O/ZnO heterostructure arrays by in situ photodeposition and application for ppb-level NO<sub>2</sub> gas sensing, *J. Alloys Compd.* 952 (2023), 169984.
- [40] P. Jin, L. Wang, X. Ma, R. Lian, J. Huang, H. She, M. Zhang, Q. Wang, Construction of hierarchical ZnIn<sub>2</sub>S<sub>4</sub>/PCN-224 heterojunction for boosting photocatalytic performance in hydrogen production and degradation of tetracycline hydrochloride, *Appl. Catal., B* 284 (2021), 119762.
- [41] J. Lee, H. Kim, T. Lee, W. Jang, K.H. Lee, A. Soon, Revisiting polytypism in hexagonal ternary sulfide ZnIn<sub>2</sub>S<sub>4</sub> for photocatalytic hydrogen production within the Z-scheme, *Chem. Mater.* 31 (2019) 9148–9155.
- [42] H. Liu, J. Xu, L. Wang, Y. Qian, H. Fu, M. Huang, X. Chen, Sensitivity enhanced and selectivity improved ethanol sensor based on ZnIn<sub>2</sub>S<sub>4</sub> nanosheet-coated In<sub>2</sub>O<sub>3</sub> nanosphere core-shell heterostructure, *J. Alloys Compd.* 898 (2022), 163000.
- [43] Y. Fan, W. Wang, H. Guan, C. Liu, X. Li, Y. Chen, J. Zhou, Y. Ma, D. Liu, S. Ruan, Sulfur vacancy-rich ZnIn<sub>2</sub>S<sub>4</sub> micro flower with 0001 facets for rapid sensing of triethylamine, *Sens. Actuators B Chem.* 374 (2023), 132826.
- [44] E. Lee, Y.S. Yoon, D.-J. Kim, Two-Dimensional transition metal dicalcogenides and metal oxide hybrids for gas sensing, *ACS Sens.* 3 (2018) 2045–2060.
- [45] S.A. Lopez-Rivera, L. Martinez, B. Fontal, W. Girit, F. Medina, Raman study of a ZnIn<sub>2</sub>S<sub>4</sub> layered compound, *Semicond. Sci. Technol.* 10 (1995) 645.
- [46] A. Compaan, H.Z. Cummins, Resonant Quadrupole-Dipole Raman Scattering at the 1S Yellow Exciton in Cu<sub>2</sub>O, *Phys. Rev. Lett.* 31 (1973) 41–44.
- [47] K.P. Ganesan, N. Anandhan, T. Marimuthu, R. Panneerselvam, A.A. Roselin, Effect of deposition potential on synthesis, structural, morphological and photoconductivity response of Cu<sub>2</sub>O thin films by electrodeposition technique, *Acta Metall. Sin. (Engl. Lett.)* 32 (2019) 1065–1074.

- [48] P.Y. Yu, Y.R. Shen, Resonance Raman studies in  $\text{Cu}_2\text{O}$ . I. The phonon-assisted 1s yellow excitonic absorption edge, *Phys. Rev. B* 12 (1975) 1377–1394.
- [49] D. Powell, A. Compaan, J.R. Macdonald, R.A. Forman, Raman-scattering study of ion-implantation-produced damage in  $\text{Cu}_2\text{O}$ , *Phys. Rev. B* 12 (1975) 20–25.
- [50] A. Živkovic, N.H. de Leeuw, B.G. Searle, L. Bernasconi, Electronic excitations in copper oxides: Time-dependent density functional theory calculations with a self-consistent hybrid kernel, *J. Phys. Chem. C* 124 (2020) 24995–25003.
- [51] Y.J. Zhang, H.M. Tang, S.-P. Gao, density functional theory study of  $\text{ZnIn}_2\text{S}_4$  and  $\text{CdIn}_2\text{S}_4$  polymorphs using full-potential linearized augmented plane wave method and modified becke–johnson potential, *Phys. Status Solidi B* 257 (2020) 1900485.
- [52] Y. Chen, G. Tian, Z. Ren, K. Pan, Y. Shi, J. Wang, F.u. Honggang, Hierarchical core-shell carbon nanofiber/ $\text{ZnIn}_2\text{S}_4$  composites for enhanced hydrogen evolution performance, *Appl. Mater. Interfaces* 6 (2014) 13841–13849.
- [53] Y.M. Choi, S.Y. Cho, D. Jang, H.J. Koh, J. Choi, C.H. Kim, H.T. Jung, Ultrasensitive Detection of VOCs Using a High-Resolution  $\text{CuO}/\text{Cu}_2\text{O}/\text{Ag}$  Nanopattern Sensor, *Adv. Funct. Mater.* 29 (2019) 1808319.
- [54] P. Li, L. Liu, D. Qin, C. Luo, G. Li, J. Hu, H. Jiang, W. Zhang,  $\text{Cu}_2\text{O}$  concave hexapod microcrystals: selective facet etching and highly improved photocatalytic performance, *J. Mater. Sci.* 54 (2019) 2876–2884.
- [55] Y. Sun, K. Suematsu, K. Watanabe, M. Nishibori, J. Hu, W. Zhang, K. Shimano, Determination of effective oxygen adsorption species for CO sensing based on electric properties of indium oxide, *J. Electrochem. Soc.* 165 (2018) B275.
- [56] H. Ali, A.C. Guler, M. Masar, P. Urbanek, M. Urbanek, D. Skoda, P. Suly, M. Machovsky, D. Galusek, I. Kuritka, Solid-state synthesis of direct Z-scheme  $\text{Cu}_2\text{O}/\text{WO}_3$  nanocomposites with enhanced visible-light photocatalytic performance, *Catalysts* 11 (2) (2021) 293.
- [57] A. Khan, M. Danish, U. Alam, S.a. Zafar, M. Munee, Facile Synthesis of a Z-Scheme  $\text{ZnIn}_2\text{S}_4/\text{MoO}_3$  Heterojunction with Enhanced Photocatalytic Activity under Visible Light Irradiation, *ACS Omega* 5 (2020) 8188–8199.
- [58] K. Khun Khun, A. Mahajan, R.K. Bedi,  $\text{SnO}_2$  thick films for room temperature gas sensing applications, *J. Appl. Phys.* 106 (2009), 124509.
- [59] D.S. Gavaskar, P. Nagaraju, P.S. Yelsani Vijayakumar, M.V. Reddy, R. Reddy, Low-cost ultra-sensitive  $\text{SnO}_2$ -based ammonia sensor synthesized by hydrothermal method, *J. Asian Ceram. Soc.* 8 (2020) 605–614.
- [60] X.W. Huang, X.B. Zou, J.Y. Shi, J.W. Zhao, Y. Li, L. Hao, J. Zhang, A new sensor for ammonia based on cyanidin-sensitized titanium dioxide film operating at room temperature, *Anal. Chim. Acta* 787 (2013) 233–238.
- [61] A. Kaur Bal, A. Singh, R.K. Bedi, Characterization and room temperature sensing of ammonia and ethanol by thermally oxidized indium films, *Phys. B* 405 (2010) 3124–3128.
- [62] G.K. Mani, J.B.B. Rayappan, A highly selective and wide range ammonia sensor nanostructured  $\text{ZnO}$ : Co thin film, *Mater. Sci. Eng. B* 191 (2015) 41–50.
- [63] F. Qu, H. Jiang, M. Yang, Designed formation through a metal-organic framework route of  $\text{ZnO}/\text{ZnCo}_2\text{O}_4$  hollow core-shell nanocages with enhanced gas sensing properties, *Nanoscale* 8 (2016) 16349–16356.
- [64] S. Bhuvaneswari, S. Papachan, N. Gopalakrishnan, Freestanding  $\text{CuO}-\text{MnO}_2$  nanocomposite for room temperature ammonia sensing, *AIP Conf. Proc.* 1832 (2017), 050126.
- [65] D.S. Asha Ramesh, P. Gavaskar, S.D. Nagaraju, S.R.K. Vanjari, C. Subrahmanyam, Mn-doped  $\text{ZnO}$  microspheres prepared by solution combustion synthesis for room temperature  $\text{NH}_3$  sensing, *Appl. Surf. Sci. Adv.* 12 (2022), 100349.
- [66] J. Zhou, M. Ikram, A.U. Rehman, J. Wang, Y. Zhao, K. Kan, W. Zhang, F. Raziq, L. Li, K. Shi, highly selective detection of  $\text{NH}_3$  and  $\text{H}_2\text{S}$  using the pristine  $\text{CuO}$  and mesoporous  $\text{In}_2\text{O}_3/\text{CuO}$  multi junctions nanofibers at room temperature, *Sens. Actuators B* 255 (2018) 1819–1830.
- [67] J. Wang, P. Yang, X. Wei, High-performance, room-temperature, and no-humidity-impact ammonia sensor based on heterogeneous nickel oxide and zinc oxide nanocrystals, *ACS Appl. Mater. Interfaces* 7 (2015) 3816–3824.